
Article:

Li, W.-B., Zhou, D. orcid.org/0000-0001-7411-4658, Xu, R. et al. (2 more authors) (2018) BaTiO3–Bi(Li0.5Ta0.5)O3, lead-free ceramics, and multilayers with high energy storage density and efficiency. ACS Applied Energy Materials, 1 (9). pp. 5016-5023. ISSN 2574-0962

https://doi.org/10.1021/acsaem.8b01001

$BaTiO_3$-$Bi(Li_{0.5}Ta_{0.5})O_3$, Lead-Free Ceramics and Multilayers with High Energy Storage Density and Efficiency

Wen-Bo Li,[a] Di Zhou[*a,b] Ran Xu,[a] Li-Xia Pang,[b,c] and Ian M. Reaney[*b]

[a]Electronic Materials Research Laboratory, Key Laboratory of the Ministry of Education & International Center for Dielectric Research, School of Electronic and Information Engineering, Xi'an Jiaotong University, Xi'an 710049, Shaanxi, China

[b]Materials Science and Engineering, University of Sheffield, S1 3JD, UK

[c]Micro-optoelectronic Systems Laboratories, Xi'an Technological University, Xi'an 710032, Shaanxi, China

[*]Corresponding author. E-mail address: zhoudi1220@gmail.com, i.m.reaney@sheffield.ac.uk

KEYWORDS: $BaTiO_3$, ceramics, multilayers, dielectrics, energy storage, capacitors.

ABSTRACT

$BaTiO_3$-based materials show great promise for energy storage capacitor but their low breakdown strength and high remnant polarization currently result in relatively low energy density. Here, we report a novel (1-x)$BaTiO_3$-xBi($Li_{0.5}Ta_{0.5}$)O_3 ($0.06 \leq x \leq 0.12$, BT-xBLT) lead-free ceramic with electric field (E) ~ 280 kV cm^{-1}, discharge energy density (W_e) ~ 2.2 J cm^{-3} , charge-discharge efficiency (η) >89% that is thermally stable up to 160 °C and with a fast discharge time (≤ 0.5 μs). Multilayers of compositions with x = 0.1 also exhibited high W_e = 4.05 J cm^{-3} and η = 95.5%, demonstrating their potential for energy storage.

1. Introduction

Capacitors with ultrahigh power density, the ultrafast discharge speed, and a wide operating temperature range have been used for energy storage applications.[1-5] They are regarded as promising energy storage devices in hybrid electric vehicles to control ripple currents.[6-8] Multilayer ceramic capacitors (MLCC) based on $BaTiO_3$ are produced in vast quantities for use as filters in computers, tablets and smart phones but their breakdown strength (E_b) and W_e are too low for applications.[9] Mass produced, low cost capacitors with high W_e would decrease volume of device.[10] High η was demanded for energy storage applications to make less waste heat causes potential dissipation problems.[11-13] High charge-discharge efficiency is important in such applications to mitigate heat dissipation problems.[14,15]

The energy storage properties of multilayers mainly depends on the defect chemistry of the dielectric.[16-18] Improving breakdown or dielectric strength, W_e and η has thus been the focus of research in this area, culminating in commercial devices based on antiferroelectric (AFE) La doped Pb(Zr,Ti)O_3 (PZT).[19,20] Jo *et al.*[19] reported the Pb-based PLZT compositions with W_{rec} of

3.04J cm^{-3} with η of 92% at 170 kV cm^{-1} but *Zhang et al.*[20] further improved properties by co-doping with Sr and Sn to give PSLZST compositions (5.56 J cm^{-3} at 350 kV cm^{-1}). However, PbO is environmentally unfriendly and is toxic to humans. Therefore, lead-free equivalents to PZT based compositions are required for high energy density storage, culminating in a number of systems being investigated such as $BaTiO_3$ (BT), $(Ba,Sr)TiO_3$ (BST), $Na_{0.5}Bi_{0.5}TiO_3$-based ceramics.[21-23] BT-based ceramics have a moderate dielectric constant are potential for energy storage capacitors. However, their low discharge energy density coupled with high remnant polarization (P_r) hinder practical applications. For BT-based ceramics dielectrics, energy density is illustrated as:

$$W = \int_0^{P_{max}} EdP \quad (1)$$

$$W_e = \int_{P_r}^{P_{max}} EdP \quad (2)$$

$$\eta = \frac{W_{rec}}{W} \times 100\% \quad (3)$$

where E is electric field. BT-based ceramics for energy storage application are thus required with a relatively high E, large P_{max} and low P_r. Therefore, optimising E and maximizing the values of (P_{max} - P_r) enhance the W_e of BT-based samples.[24-28] Oxides which are known to have intrinsically high dielectric strength such as Al_2O_3, SiO_2 and MgO have been introduced into the BT-based ceramics to enhance the breakdown voltage and energy storage properties.[24-26] BT based ceramics formed from Al_2O_3- and SiO_2-coated powders show higher breakdown strength (190 kV cm^{-1}) which gives rise to higher W_e = 0.725 J cm^{-3} and greater η ~ 80%.[23] $BaSrTiO_3$-MgO composites were prepared by using a new preparation method (SPS) to obtain breakdown

strength 300 kV cm^{-1}, W_e ~ 1.5 J cm^{-3} and η ~ 88.5%.[25] Recent studies have shown that Bi^{3+} modified $BaTiO_3$ ceramics own high W_e due to their large P_{max} and small P_r. $BaTiO_3$-$BiMeO_3$ systems have been studied widely with $0.7BaTiO_3$-$0.3BiScO_3$ capacitors exhibiting remarkably high W_e of 6.1 J cm^{-3} but under extremely high electric field, 730 kV cm^{-1}.[26] $0.75(Bi_{0.75}Nd_{0.15})FeO_3$-$0.25BaTiO_3$-0.1wt% MnO_2 ceramics have been shown to exhibit high W_{rec} (1.81 J cm^{-3}) and low η (41.3%) but multilayers of the same composition demonstrated significant improvement in performance.[27] In contrast, Shen *et al.* reported $0.91BaTiO_3$-$0.09BiYbO_3$ ceramics with high W_e ~ 0.71 J cm^{-3} and further work on relaxor compounds in the solid solutions $BaTiO_3$-$BiB^{3+}O_3$ (B = Y, Sc, Ga, Al, In), $BaTiO_3$-$Bi(Mg_{2/3}Nb_{1/3})O_3$ and $BaTiO_3$-$Bi(Mg_{1/2}Ti_{1/2})O_3$ revealed W_e typically limited to <1.85 J cm^{-3}.[28-32] Despite the disappointing values of W_e, BT based relaxor-ferroelectrics hold promise for energy storage and inspired the design and synthesis of 0.88BT-0.12BLN ceramic, which exhibited one of the highest energy density (2.013 J cm^{-3} under 270 kV cm^{-1}) in lead free ceramics.[33] Most importantly, it indicated that Bi^{3+} ion inter into the Ba site could optimize the W_e by maximizing P_{max} and minimising P_r.[34,35] In this contribution, a further relaxor ferroelectrics BT-*x*BLT ($0.06 \leq x \leq 0.12$) was designed with enhanced E ~ 280 kV cm^{-1}, W_e ~ 2 J cm^{-3} and η ~ 88%. Multilayers of the ceramic compositions also exhibited promising properties with E ~ 466 kV cm^{-1}, W_e ~ 4.05 J cm^{-3} and η ~ 95.5%.

2. Results and discussion

Figure 1a shows the XRD traces of BT-*x*BLT ($0.06 \leq x \leq 0.12$) samples. All peaks of BT-xBLT ceramics are indexed according to a cubic perovskite phase, indicating solid solubility up to at least $x = 0.12$. Fig. 1b shows the variation of cell parameters and the volume of the BT-*x*BLT ceramics and Rietveld refinement fitting of 0.90BT-0.10BLT, respectively. From Fig. 1b,

cell parameters and the volume increase from 4.0117(1) to 4.0152(2) Å and 64.563(5) to 64.736(5) $Å^3$ with the *x* values increase from 0.06 to 0.12, respectively. According to the Shannon's ionic radii (R), R of Ba^{2+} (1.61 Å, 12 fold coordination) in the ABO_3 perovskite structure is larger than Bi^{3+} (1.35 Å).[36] The average ionic radii of $(Li_{0.5}Ta_{0.5})^{3+}$ is 0.70 Å[36] and similar to but slightly larger than Ti^{4+} (0.605 Å). We propose therefore that Bi^{3+} and $(Li_{0.5}Ta_{0.5})^{3+}$ enter the Ba and Ti site, respectively. XRD patterns were refined with space group Pm-3m (No. 221). Fig. S1 exhibited the results of fitted XRD patterns of BT-*x*BLT. The results of refined crystal structure and related parameters are also listed in Table S1. Fig. 1c shows Rietveld refinement fitting of 0.90BT-0.10BLT ceramic with all reflections indexed and with a satisfactory 'goodness of fit' (R_p= 6.74%, R_{wp}= 9.02% and R_{exp}= 5.95%). Refined fractional coordinates of Ba^{2+}, Bi^{3+}, Li^{+}, Ta^{5+}, Ti^{4+} ions are shown in Table 1 with $a = b = c$ = 4.0139 (2) Å, (Ba^{2+} and Bi^{3+}) and (Li^{+}, Ta^{5+} and Ti^{4+}) randomly distributed at the 1a Wyckoff position 1b respectively. Meantime, oxygen occupying 3c. A <110> SAED pattern of 0.90BT-0.10BLT is also shown in the inset of Fig. 1c which confirms the absence of superstructure reflections, consistent with Pm-3m symmetry.

Figure 2 a, c, e and g show SEM images of thermal etching surfaces, respectively for 0.94BT-0.06BLT, 0.92BT-0.08BLT, 0.90BT-0.10BLT and 0.88BT-0.12BLT samples. All samples exhibit a dense microstructure and no porosity. Distribution histograms from BT-*x*BLT (Fig 2b, d, f and h) show an average grain size of 0.6, 0.8, 1.2, and 1.6 for x = 0.06, 0.08, 0.10, and 0.12, respectively.

Figure 3 exhibits the location distribution of ions in 0.90BT-0.10BLT ceramic by using the elemental mapping. In Fig. 3a, it shows that these ions are uniformly distributed on top of the

grain and do not aggregate at the grain boundary. The ions of 0.90BT-0.10BLT ceramic are similar molar ratios to the batched 0.90BT-0.10BLT composition, Fig. 3b.

Figure 4 shows dielectric constant (ε_r) and dielectric loss (*tanδ*) of BT-BLT samples in temperature range -90 to 110 °C from 100 Hz to 1 MHz. ε_r decreased from 1980 for 0.94BT-0.06BLT to 760 for 0.88BT-0.12BLT ceramics accompanied by a low *tanδ* (< 0.01) at room temperature. Previous studies have reported that $BiM_1M_2O_3$ substitution in $BaTiO_3$ mitigates sintering temperature and dielectric loss.[24-26] with BT-BLT ceramics following similar trends. Fig. S2 exhibits Frequency dependence of ε_r and *tanδ* of the BT-BLT ceramics at 25 °C is shown in. ε_r decreases as frequency increases from 1 kHz ~ 10 MHz consistent with a dielectric relaxation widely observed in related $BaTiO_3$-$BiMeO_3$ systems.[24-26]

From Fig. 5a, the electrical resistivity of BT-BLT increased with increasing BLT concentration to maximum at x = 0.10. Breakdown strength (E_b) is key to optimizing energy storage density and therefore it is critical to have a robust methodology to establish this metric. To this end, the results of E_b are analysed by using the Weibull distribution function in Fig. 5b. From Fig. 5b, it can be seen all results of E_b fit well with the Weibull distribution for the samples. The characteristic E_b of 0.94BT-0.06BLT, 0.92BT-0.08BLT, 0.90BT-0.10BLT and 0.88BT-0.12BLT samples are therefore 290, 330, 335, and 332 kV cm^{-1}, respectively. The highest characteristic E_b can be achieved in the 0.9BT-0.1BLT ceramic with high resistivity about 3.53×10^{12} Ω cm. Compared with other $BaTiO_3$-based samples, the values of E_b are significantly improved.[28-36] Fig. S3 shows polarization-electric field (P-E) hysteresis of BT-xBLT ceramics measured with unipolar triangle signals at 10 Hz near the breakdown voltage. The P-E hysteresis of BT-xBLT samples transform gradually from a saturated loop to slim loops as x increased. From Fig. S3, breakdown strength of BT-BLT ceramics increases from 175 to

280 kV cm^{-1} but then reduces to 225 kV cm^{-1} with increase in BLT concentration and is significantly greater than most BT-based bulk ceramics.[28-36] The W_e of the BT-BLT samples was measured by using P-E hysteresis loops in Fig. S3a. Fig. 5c illustrates the W_e and η as a function of BLT concentration. Although the W_e increases and reaches a maximum but then decreases with increase in BLT concentration, the η continuously increase from $0.06 \leq x \leq 0.12$. Outstanding energy storage performance of 0.90BT-0.10BLT is about $W_e \sim 2.2$ J cm^{-3} and $\eta \sim$ 88.1% under 280 kV cm^{-1}. Fig. S3b shows P-E hysteresis loops of the 0.90BT-0.10BLT ceramic under various E at 25 °C. Based on P-E hysteresis loops of 0.90BT-0.10BLT sample in Fig. S3b, the result of the high performance of ceramic is exhibited in Fig. 5d. When electric field adds from 40 to 280 kV cm^{-1}, the W_e increases from 0.21 J cm^{-3} to 2.2 J cm^{-3} while the η is consistently > 88%.

For the capacitors in practical use, the discharge speed is required as fast as possible for pulsed power applications. It usually defined the $\tau_{0.9}$ as the discharge time to evaluate discharge speed. The $\tau_{0.9}$ means the time it takes to release 90% of energy value in the circuit.[51-53] It is important to study the discharge process by using a capacitor discharge circuit (Fig. S4). In this study, the discharge processes of the BT-xBLT capacitors are measured by load resistor of 205 Ω. Fig. 6 shows the discharging rate of BT-xBLT ceramics at 150 kV cm^{-1}. Fig. 6 exhibits the variation of discharge current waveforms and W_e on discharge time. The $\tau_{0.9}$ of the 0.94BT-0.06BLT, 0.92BT-0.08BLT, 0.90BT-0.10BLT and 0.88BT-0.12BLT ceramics are about 0.25 μs, 0.28 μs, 0.32 μs, 0.34 μs in the discharge processes.

In general, the ambient temperature of electronic device is up to 160 °C.[32] So thermal stability is very important for electronic materials.[33] Fig. S5 shows *P-E* loops of BT-xBLT from 25 to 160 °C under same electric field of 150 kV cm^{-1} with BT-xBLT ceramics generally

exhibiting slim P-E loops. Fig. 7 shows P_r, P_{max} and energy storage properties of BT-xBLT ceramics in from 25 to 160 °C. P_r and P_{max} decreased only slightly at 160 °C, compared with room temperature, as shown in Fig. 7a, indicating that polarization response is almost independent of temperatures. Fig. 7b exhibits the variation of W_e and η with temperature. Only slight variation in W_e coupled with a high η is observed up 160 °C.

To further illustrate the potential of the BT-xBLT system for energy storage applications, 0.90BT-0.10BLT multilayers with Pt internal electrode were prepared by the tape-casting (see Supporting Information). Fig. 8a shows SEM images of a 0.90BT-0.10BLT multilayer with a dielectric layer thickness of ~ 30 μm. Fig. 8b exhibits *P-E* hysteresis of the 0.90BT-0.10BLT multilayer under varying E at 25 °C. High E_b ~ 466 kV cm^{-1} is observed, favourable for high W_e which along with the slim P-E loops is expected to give rise to high energy storage density. The studies have been shown that high η is demanded of multilayers in energy storage applications as waste heat causes potential dissipation problems in the charge-discharge progress.[35-39] Fig. 8c shows the W_e and η of 0.90BT-0.10BLT multilayers at various electric fields. The W and W_e of 0.90BT-0.10BLT multilayers increased from 0.59 and 0.63 to 4.05 and 4.24 J cm^{-3}, respectively, with the E enhanced from 120 to 466 kV cm^{-1}. In addition, high η (95.5%) was obtained for the 0.90BT-0.10BLT multilayers at high breakdown voltages (466 kV cm^{-1}). High η mitigates potential heat dissipation problems.[13-16] Finally, Fig. 8d compares the W_e, E_b, and η of this work with other outstanding lead free systems which illustrates that 0.90BT-0.10BLT ceramics and multilayers have a combination of energy density, breakdown strength, and efficiency superior to other lead free systems.

3. Conclusion

In summary, we reported novel high E_b and W_e of the BT-xBLT ceramics and multilayers. This work significantly improved energy storage capacity of BT-BLT system (W_e ~ 4.05 J cm^{-3} and η ~ 95.5%) than other $BaTiO_3$-based systems (W_e < 2 J cm^{-3} and η ~ 80%). All samples densified at 1200 ~ 1260 ^{o}C with XRD demonstrated that a solid solution had been formed. The 0.90BT-0.10BLT ceramics had high E_b ~ 280 kV cm^{-1}, W_e ~ 2.2 J cm^{-3}, η ~ 88%, temperature stability from ~25 ^{o}C to ~ 160 ^{o}C with a fast release speed ($\tau_{0.9} \leq 0.50$ μs). Meanwhile, the 0.90BT-0.10BLT multilayers were fabricated with ultra-high energy density ~ 4.05 J cm^{-3} and η ~95.5% under 466 kV/cm, which confirmed that lead-free BT-BLT systems are promising alternative for applications in high energy density storage.

Figure Captions:

Figure 1. (a) XRD patterns of the BT-xBLT ceramics. (b) Variation cell parameters of the BT-xBLT ceramics. (c) Rietveld profile fitting of 0.90BT-0.10BLT. The open circles show experimental and the continuous curve shows the best fit to the XRD pattern with a cubic Pm-3m space group. Insets give the perovskite structure of ABO_3 and SAED.

Figure 2. SEM images of thermally etched surfaces and grain size distribution histograms for the BT-xBLT ceramics: (a)-(b) 0.94BT-0.06BLT, (c)-(d) 0.92BT-0.08BLT, (e)-(f) 0.90BT-0.10BLT, (g)-(h) 0.88BT-0.12BLT.

Figure 3. (a) Element mapping images of 0.90BT-0.10BLT sintered at optimum temperature and (b) EDX chemical mapping: blue, O-K; cyan, Bi-M; olive, Ba-L; green, Ti-K; and red, Ta-L.

Figure 4. Relative permittivity and loss tangent of BT-xBLT ceramics as a function of temperature (-90 °C to 110 °C) from 100 Hz to 1 MHz: (a) 0.94BT-0.06BLT, (b) 0.92BT-0.08BLT, (c) 0.90BT-0.10BLT, (d) 0.88BT-0.12BLT.

Figure 5. (a) Electrical resistivity of BT-xBLT ceramics. (b) Weibull distributions of E_b of BT-xBLT ceramics. (c) W_e and η of BT-xBLT ceramics near their breakdown strength. (d) The W, W_e and η of 0.90BT-0.10BLT ceramic at various electric fields.

Figure 6. (a) Pulsed discharging current of BT-xBLT samples at same electric field of 150 kV cm^{-1}. (b) The W_e of BT-xBLT samples depending on discharging time.

Figure 7. (a) The P_r and P_{max} for BT-xBLT ceramics at different temperatures. (b) The W_e and η of BT-xBLT ceramics depending on temperatures.

Figure 8. (a) SEM images of 0.90BT-0.10BLT MLCC samples. (b) The P-E hysteresis of 0.90BT-0.10BLT MLCC samples at 466 kV cm^{-1} at 25 ^{o}C. (c) Variation of the W, W_e and η of 0.90BT-0.10BLT MLCC samples depending on electric field. (d) Comparison of the W_e and η of 0.90BT-0.10BLT MLCC samples and other lead-free ceramic systems: BT-BLN ($BaTiO_3$-$Bi(Li_{1/2}Nb_{1/2})O_3$)[33]; BT-BMT ($BaTiO_3$-$Bi(Mg_{1/2}Ti_{1/2})O_3$)[26]; BST ($Ba_{0.4}Sr_{0.6}TiO_3$)[20]; BT-BMN ($BaTiO_3$-$Bi(Mg_{2/3}Nb_{1/3})O_3$)[25]; BT-BI ($BaTiO_3$-$BiInO_3$)[33]; BT-BZN ($BaTiO_3$-$Bi(Zn_{2/3}Nb_{1/3})O_3$)[23]; BT-BZT ($BaTiO_3$-$Bi(Zn_{1/2}Ti_{1/2})O_3$)[33]; BT-BS ($BaTiO_3$@$BiScO_3$)[37]; BT-BYb ($BaTiO_3$-$BiYbO_3$)[22]; BT-BY ($BaTiO_3$-$BiYO_3$)[37]; BLNLTZ-NBN ($Na_{0.73}Bi_{0.09}NbO_3$-$Bi_{0.48}La_{0.02}Na_{0.48}Li_{0.02}Ti_{0.98}Zr_{0.02}O_3$)[42]; BT-NBT-NBN ($BaTiO_3$-$Bi_{0.5}Na_{0.5}TiO_3$-$Na_{0.73}Bi_{0.09}NbO_3$)[35]; NBBT-BMT ($(Na_{0.5}Bi_{0.5})_{0.92}Ba_{0.08}TiO_3$-$Bi(Mg_{0.5}Ti_{0.5})O_3$)[34]; NBT-KN ($Na_{0.5}Bi_{0.5}TiO_3$-$KNbO_3$)[46]; NBBT-KN ($Na_{0.47}Bi_{0.47}Ba_{0.06}TiO_3$-$KNbO_3$)[46]; NBT-BT-SZ-NN ($Bi_{0.5}Na_{0.5}TiO_3$-$BaTiO_3$-$SrZrO_3$-$NaNbO_3$)[36]; NBABT ($Na_{0.42}Bi_{0.44}Al_{0.06}Ba_{0.08}TiO_3$)[38]; AN ($AgNbO_3$)[50]. Red and blue bars correspond to energy density and electric field.

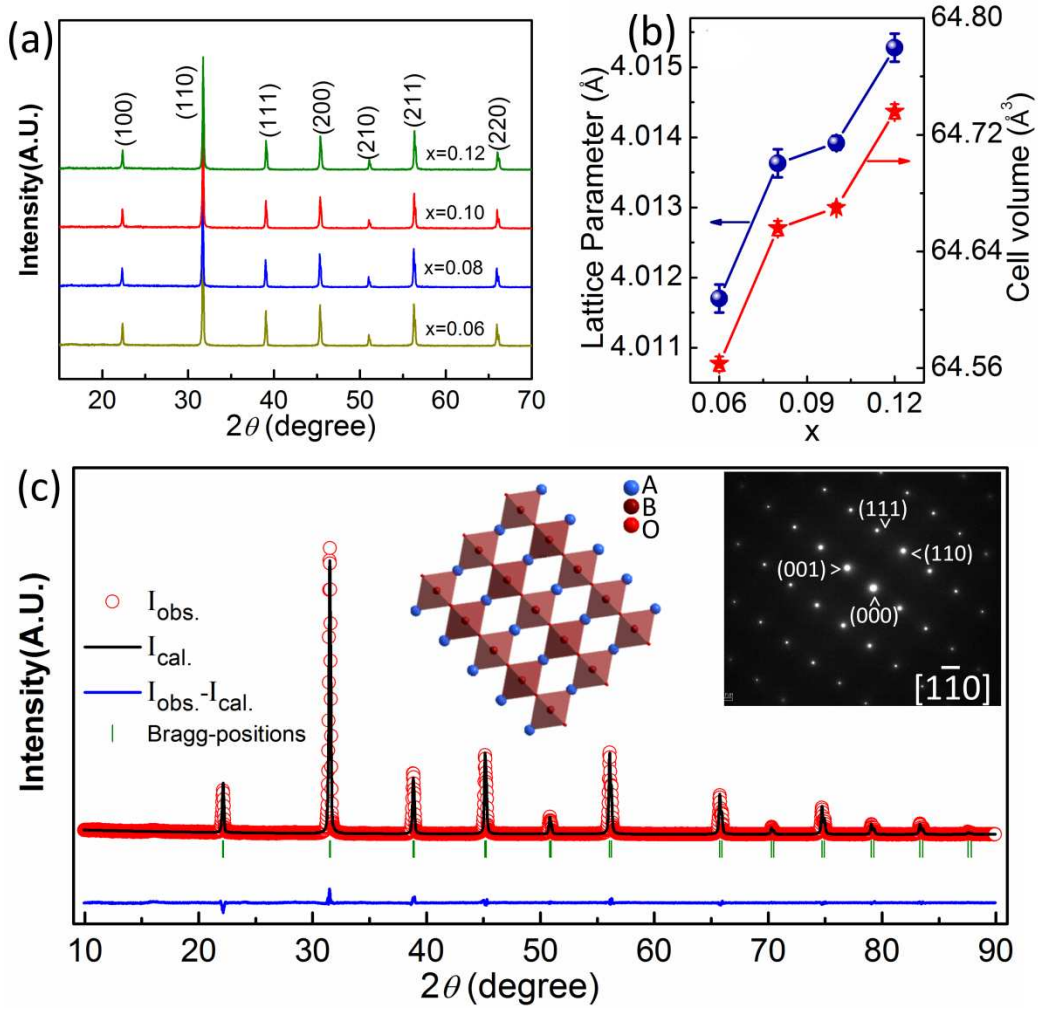

Figure 1. (a) XRD patterns of the BT-xBLT ceramics. (b) Variation cell parameters of the BT-xBLT ceramics. (c) Rietveld profile fitting of 0.90BT-0.10BLT. The open circles show experimental and the continuous curve shows the best fit to the XRD pattern with a cubic Pm-3m space group. Insets give the perovskite structure of ABO_3 and SAED.

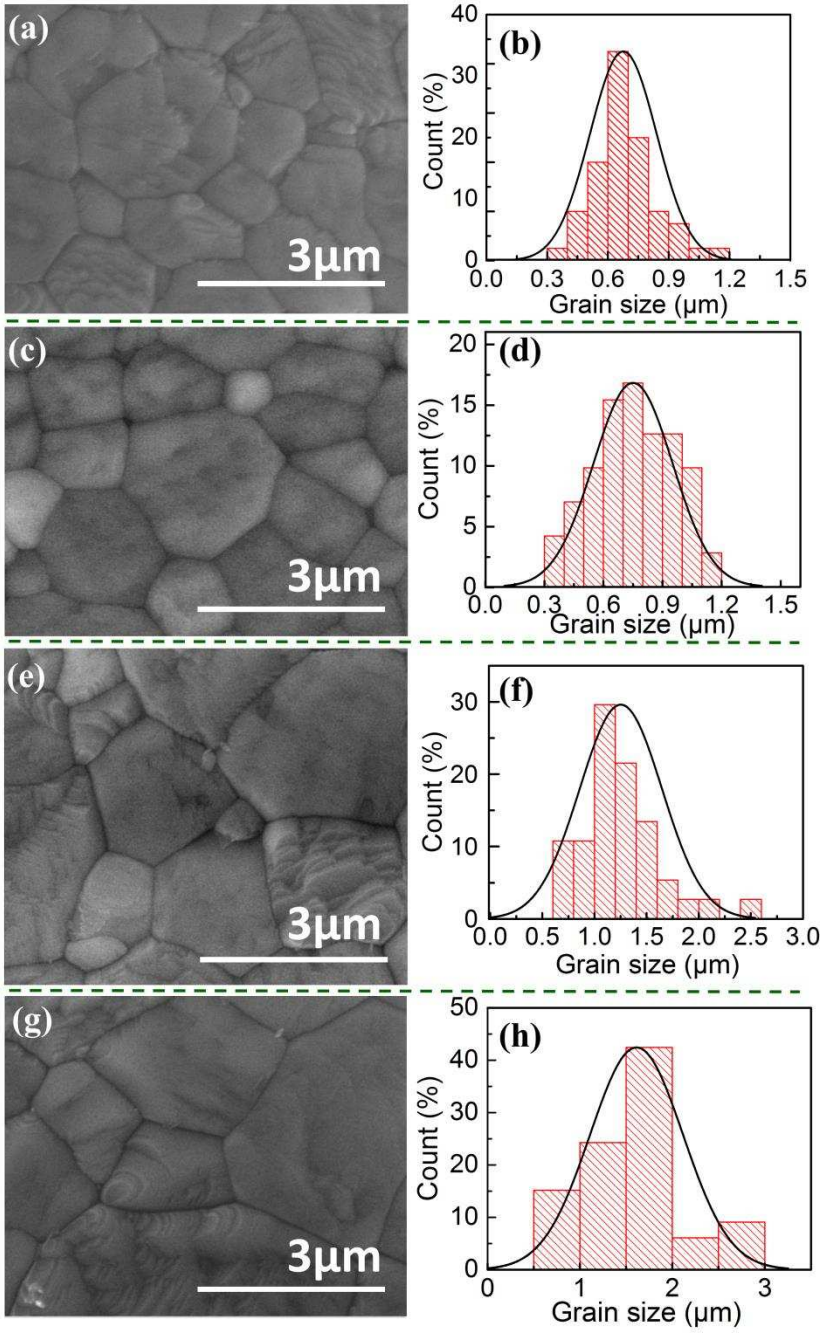

Figure 2. SEM images of thermally etched surfaces and grain size distribution histograms for the BT-xBLT ceramics: (a)-(b) 0.94BT-0.06BLT, (c)-(d) 0.92BT-0.08BLT, (e)-(f) 0.90BT-0.10BLT, (g)-(h) 0.88BT-0.12BLT.

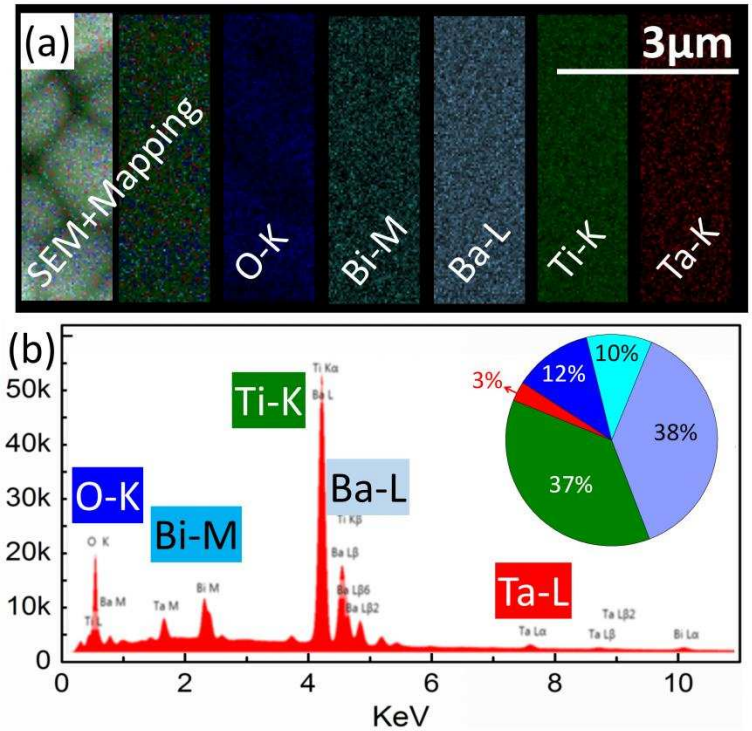

Figure 3. (a) Element mapping images of 0.90BT-0.10BLT sintered at optimum temperature and (b) EDX chemical mapping: blue, O-K; cyan, Bi-M; olive, Ba-L; green, Ti-K; and red, Ta-L.

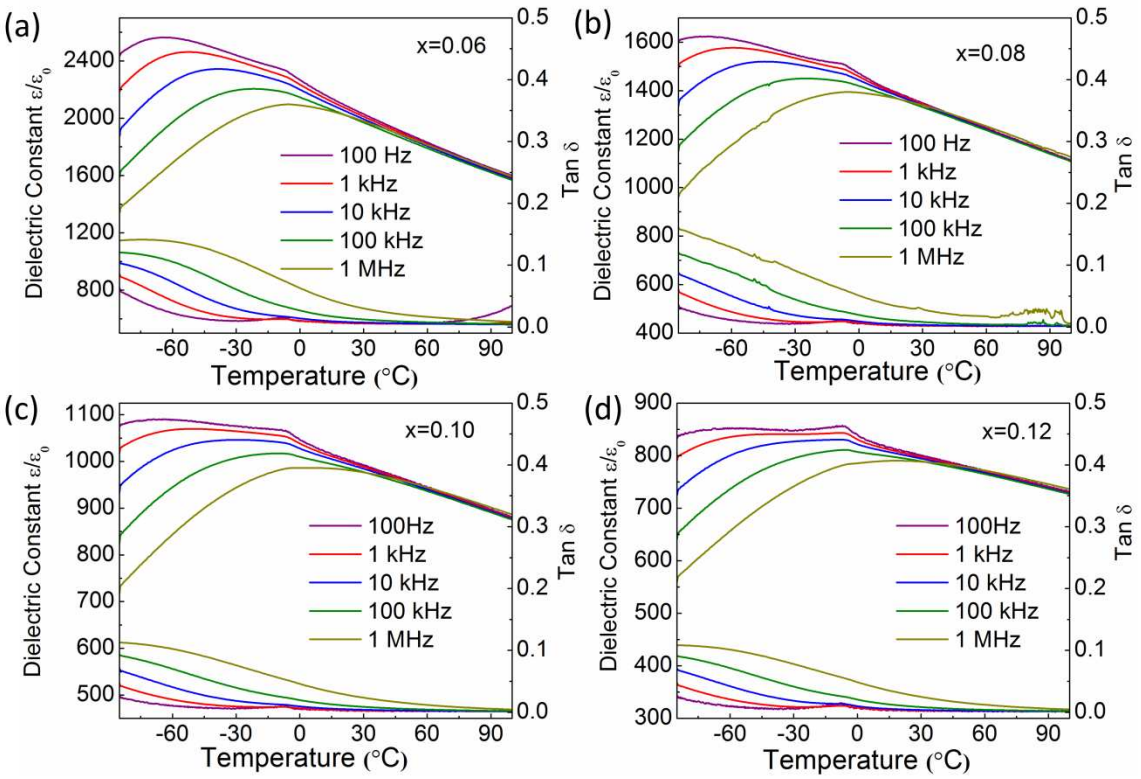

Figure 4. Relative permittivity and loss tangent of BT-xBLT ceramics as a function of temperature (-90 °C to 110 °C) from 100 Hz to 1 MHz: (a) 0.94BT-0.06BLT, (b) 0.92BT-0.08BLT, (c) 0.90BT-0.10BLT, (d) 0.88BT-0.12BLT.

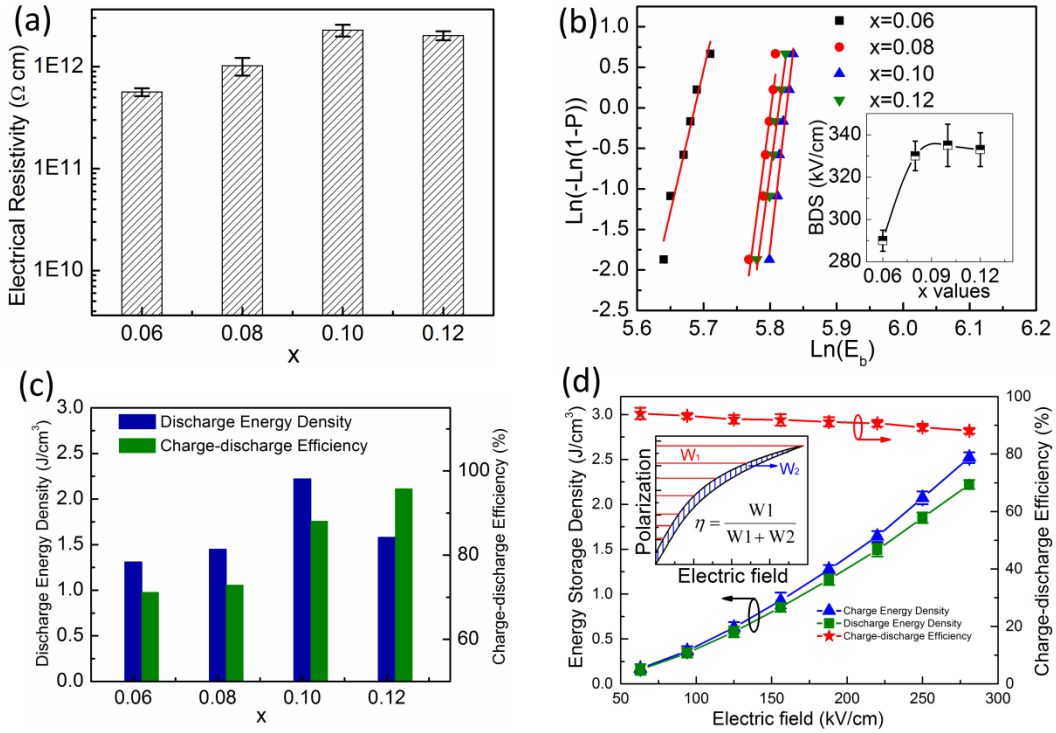

Figure 5. (a) Electrical resistivity of BT-xBLT ceramics. (b) Weibull distributions of E_b of BT-xBLT ceramics. (c) W_e and η of BT-xBLT ceramics near their breakdown strength. (d) The W, W_e and η of 0.90BT-0.10BLT ceramic at various electric fields.

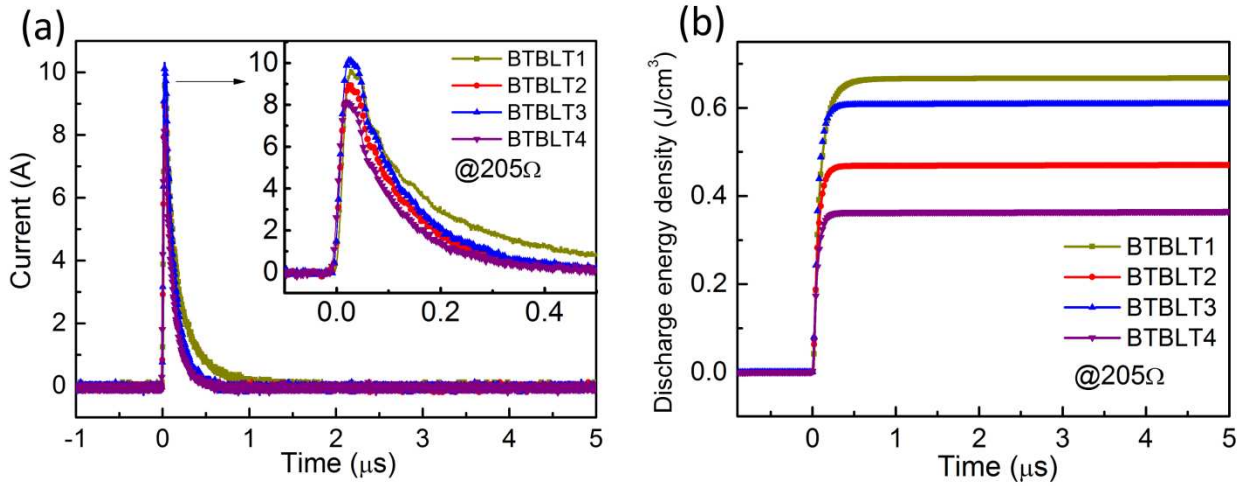

Figure 6. (a) Pulsed discharging current of BT-xBLT samples at same electric field of 150 kV cm^{-1}. (b) The W_e of BT-xBLT samples depending on discharging time.

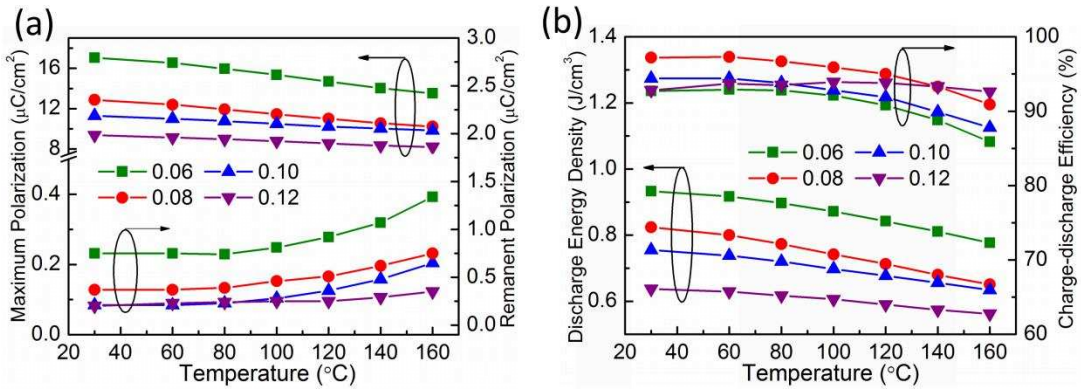

Figure 7. (a) The P_r and P_{max} for BT-xBLT ceramics at different temperatures. (b) The W_e and η of BT-xBLT ceramics depending on temperatures.

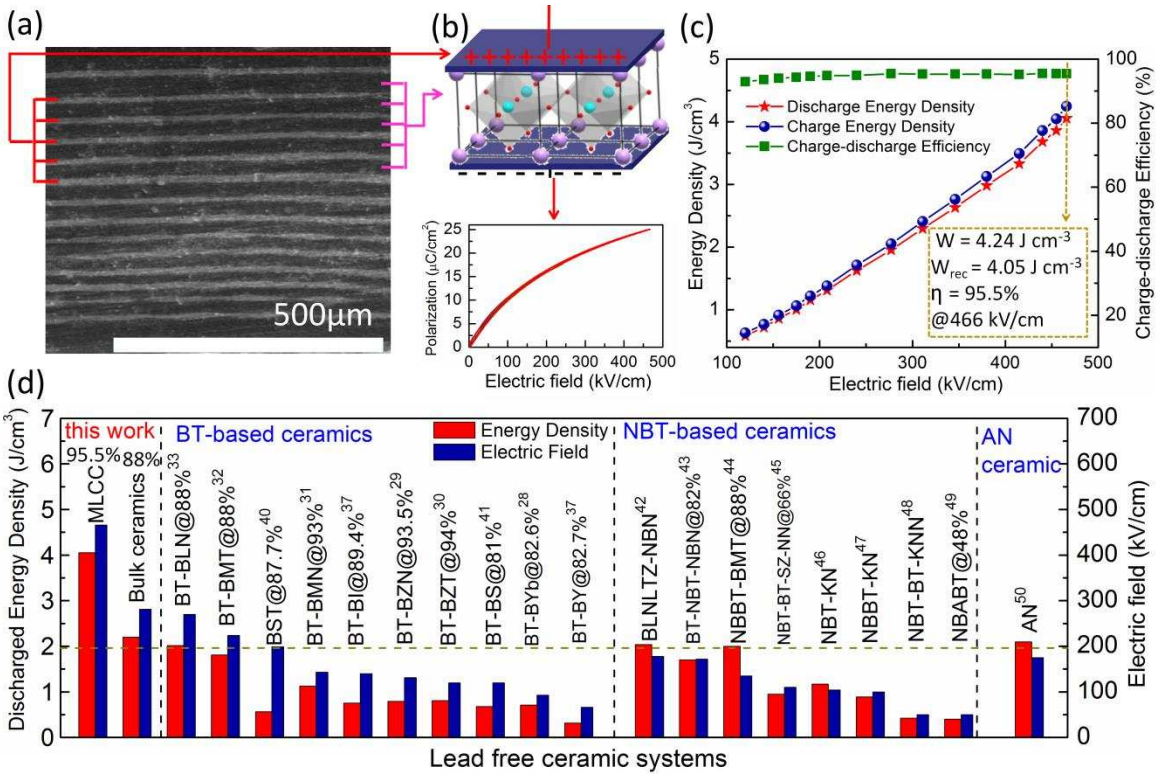

Figure 8. (a) SEM images of 0.90BT-0.10BLT MLCC samples. (b) The P-E hysteresis of 0.90BT-0.10BLT MLCC samples at 466 kV cm^{-1} at 25 °C. (c) Variation of the W, W_e and η of 0.90BT-0.10BLT MLCC samples depending on electric field. (d) Comparison of the W_e and η of 0.90BT-0.10BLT MLCC samples and other lead-free ceramic systems: BT-BLN ($BaTiO_3$-$Bi(Li_{1/2}Nb_{1/2})O_3$)[33]; BT-BMT ($BaTiO_3$-$Bi(Mg_{1/2}Ti_{1/2})O_3$)[32]; BST ($Ba_{0.4}Sr_{0.6}TiO_3$)[40]; BT-BMN ($BaTiO_3$-$Bi(Mg_{2/3}Nb_{1/3})O_3$)[31]; BT-BI ($BaTiO_3$-$BiInO_3$)[37]; BT-BZN ($BaTiO_3$-$Bi(Zn_{2/3}Nb_{1/3})O_3$)[29]; BT-BZT ($BaTiO_3$-$Bi(Zn_{1/2}Ti_{1/2})O_3$)[30]; BT-BS ($BaTiO_3$@$BiScO_3$)[41]; BT-BYb ($BaTiO_3$-$BiYbO_3$)[28]; BT-BY ($BaTiO_3$-$BiYO_3$)[37]; BLNLTZ-NBN ($Na_{0.73}Bi_{0.09}NbO_3$-$Bi_{0.48}La_{0.02}Na_{0.48}Li_{0.02}Ti_{0.98}Zr_{0.02}O_3$)[42]; BT-NBT-NBN ($BaTiO_3$-$Bi_{0.5}Na_{0.5}TiO_3$-$Na_{0.73}Bi_{0.09}NbO_3$)[43]; NBBT-BMT ($(Na_{0.5}Bi_{0.5})_{0.92}Ba_{0.08}TiO_3$-$Bi(Mg_{0.5}Ti_{0.5})O_3$)[44]; NBT-KN ($Na_{0.5}Bi_{0.5}TiO_3$-$KNbO_3$)[46]; NBBT-KN ($Na_{0.47}Bi_{0.47}Ba_{0.06}TiO_3$-$KNbO_3$)[47]; NBT-BT-SZ-NN ($Bi_{0.5}Na_{0.5}TiO_3$-$BaTiO_3$-$SrZrO_3$-$NaNbO_3$)[45]; NBABT ($Na_{0.42}Bi_{0.44}Al_{0.06}Ba_{0.08}TiO_3$)[49]; AN ($AgNbO_3$)[50]. Red and blue bars correspond to energy density and electric field.

TABLES.

Table 1. Refined structural parameters from XRD Data for the 0.90BT-0.10BLT Sample.

Atom	Site	Occ.	x	y	z	Biso.
Ba1	1a	0.300	0.0000	0.0000	0.0000	1.5073(8)
Bi1	1a	0.033	0.0000	0.0000	0.0000	1.5073(8)
Ti1	1b	0.300	0.5000	0.5000	0.5000	0.0986(1)
Li1	1b	0.017	0.5000	0.5000	0.5000	0.0986(1)
Ta1	1b	0.017	0.5000	0.5000	0.5000	0.0986(1)
O1	3c	1.000	0.5000	0.5000	0.0000	0.0921(1)

a = b=c = 4.0139 (2) Å. R_p~ 6.74, R_{wp}~ 9.02, R_{exp}~ 5.95

ASSOCIATED CONTENT

Supporting Information.

Experimental Section; Preparation of the MLCC samples; crystal and refinement parameters for BT-xBLT; rietveld profile fitting of BT-xBLT for x = 0.06, 0.08, 0.10 and 0.12; the P-E hysteresis of BT-xBLT ceramics near their breakdown strength; The P-E hysteresis of 0.90BT-0.10BLT ceramic at room temperatures as a function of electric fields; the P-E hysteresis of BT-xBLT ceramics at RT to 160 ^{o}C; the schematic diagram for pulsed discharging current.

AUTHOR INFORMATION

Corresponding Author

*E-mail: zhoudi1220@gmail.com.

*E-mail: i.m.reaney@sheffield.ac.uk.

Notes

The authors declare no competing financial interest.

ACKNOWLEDGMENT

This work was supported by the National Natural Science Foundation of China (U1632146), the Young Star Project of Science and Technology of Shaanxi Province (2016KJXX-34), the Key Basic Research Program of Shaanxi Province (2017GY-129), the Fundamental Research Funds for the Central University, and the 111 Project of China (B14040). The SEM and EDX work was done at International Center for Dielectric Research (ICDR), Xi'an Jiaotong University, Xi'an, China and the authors thank Ms. Yan-Zhu Dai for her help in using SEM and EDX. Ian Reaney

and Di Zhou would also like to acknowledge the Engineering and Physical Science Research Council grant EP/L017563/1 for support.

REFERENCES

(1) Love, G. R. Energy-Storage in Ceramic Dielectrics. J. Am. Ceram. Soc. **1990**, 73, 323-328.

(2) Zhang, Q. M.; Li, H. F.; Poh, M.; Xu, H. S.; Cheng, Z. Y.; Xia, F.; Huang, C. An All-Organic Composite Actuator Material with A High Dielectric Constant. Nature **2002**, 419, 284-287.

(3) Chu, B.; Zhou, X.; Ren, K.; Neese, B.; Lin, M.; Wang, Q.; Bauer, F.; Zhang, Q. M. A Dielectric Polymer with High Electric Energy Density and Fast Discharge Speed. Science **2006**, 313, 334-336.

(4) Li, Q.; Chen, L.; Gadinski, M. R.; Zhang, S. H.; Zhang, G. Z.; Li, H. Y.; Haque, A.; Chen, L. Q.; Jackson, T.; Wang, Q. Flexible High Temperature Dielectric Materials from Polymer Nanocomposites. Nature **2015**, 523, 576-579.

(5) Hu, W. B.; Liu, Y.; Withers, R. L.; Frankcombe, T. J.; Norén, L.; Snashall, A.; Kitchin, M.; Smith, P.; Gong, B.; Chen, H.; Schiemer, J.; Brink, F.; Leung, J. W. Electron-Pinned Defect-Dipoles for High-Performance Colossal Permittivity Materials. Nature Mater. **2013**, 12, 821-826.

(6) Luo, S.; Shen, Y.; Yu, S.; Wan, Y.; Liao, W. H.; Sun, R.; Wong C. P. Construction of A 3D-$BaTiO_3$ Network Leading to Significantly Enhanced Dielectric Permittivity and Energy Storage Density of Polymer Composites. Energy Environ. Sci. **2017**, 10, 137-144.

(7) Li, Q.; Zhang, G.; Liu, F.; Han, K.; Gadinski, M. R.; Xiong, C.; Wang, Q. Solution-Processed Ferroelectric Terpolymer Nanocomposites with High Breakdown Strength and Energy Density Utilizing Boron Nitride Nanosheets. Energy Environ. Sci. **2015**, 8, 922-931.

(8) Yang, H.; Yan, F.; Lin, Y.; Wang, T. Novel Strontium Titanate-Based Lead-Free Ceramics for High-Energy Storage Applications. ACS Sustainable Chem. Eng. **2017**, 5, 10215-10222.

(9) Tang, H.; Lin, Y.; Sodano, H. A. Synthesis of High Aspect Ratio $BaTiO_3$ Nanowires for High Energy Density Nanocomposite Capacitors. Adv. Energy Mater. **2013**, 3, 451-456.

(10) Yan, F.; Yang, H.; Lin, Y.; Wang, T. Dielectric and Ferroelectric Properties of $SrTiO_3$-$Bi_{0.5}Na_{0.5}TiO_3$-$BaAl_{0.5}Nb_{0.5}O_3$ Lead-Free Ceramics for High-Energy-Storage Applications. Inorg. Chem. **2017**, 56, 13510-13516.

(11) Yao, Z.; Song, Z.; Hao, H.; Yu, Z.; Cao, M.; Zhang, S.; Lanagan, M.T.; Liu, H. Homogeneous/Inhomogeneous-Structured Dielectrics and their Energy-Storage Performances. Adv. Mater. **2017**, 29, 1601727.

(12) Song, Z.; Liu, H.; Zhang, S.; Wang, Z.; Shi, Y.; Hao, H.; Cao, M.; Yao, Z.; Yu, Z. Effect of Grain Size on The Energy Storage Properties of $(Ba_{0.4}Sr_{0.6})TiO_3$ Paraelectric Ceramics. J. Eur. Ceram. Soc. **2014**, 34,1209-1217.

(13) Zhang, X.; Shen, Y.; Shen, Z.; Jiang, J.; Chen, L.; Nan, C. W. Achieving High Energy Density in PVDF-Based Polymer Blends: Suppression of Early Polarization Saturation and Enhancement of Breakdown Strength. ACS Appl. Mater. Interfaces **2016**, 8, 27236-27242.

(14) Tang, H.; Sodano, H. A. Ultra High Energy Density Nanocomposite Capacitors with Fast Discharge Using $Ba_{0.2}Sr_{0.8}TiO_3$ Nanowires. Nano Lett. **2013**, 13, 1373-1379.

(15) Sun, Z.; Ma, C.; Wang, X.; Liu, M.; Lu, L.; Wu, M.; Lou, X.; Wang, H.; Jia, C. L. Large Energy Density, Excellent Thermal Stability, and High Cycling Endurance of Lead-Free $BaZr_{0.2}Ti_{0.8}O_3$ Film Capacitors. ACS Appl. Mater. Interfaces **2017**, 9, 17096-17101.

(16) Zhang, X.; Shen, Y.; Xu, B.; Zhang, Q. H.; Gu, L.; Jiang, J. Y.; Ma, J.; Lin, Y. H.; Nan, C. W. Giant Energy Density and Improved Discharge Efficiency of Solution-Processed Polymer Nanocomposites for Dielectric Energy Storage. Adv. Mater. **2016**, 28, 2055-2061.

(17) Tian, Y.; Jin, L.; Zhang, H.; Xu, Z.; Wei, X.; Viola, G.; Abrahams, I.; Yan, H. Phase Transitions in Bismuth-Modified Silver Niobate Ceramics for High Power Energy Storage. J. Mater. Chem. A **2017**, 5, 17525-17531.

(18) Park, M. H.; Lee, Y. H.; Kim, H. J.; Kim, Y. J.; Moon, T.; Kim, K. D.; Müller, J.; Kersch, A.; Schroeder, U.; Mikolajick, T.; Hwang, C. S. Ferroelectricity and Antiferroelectricity of Doped Thin HfO_2-Based Films. Adv. Mater. **2015**, 27, 1811-1831.

(19) Jo, H. R.; Lynch, C. S. A High Energy Density Relaxor Antiferroelectric Pulsed Capacitor Dielectric. J. Appl. Phys. **2016**, 119, 024104.

(20) Zhang, Q. F.; Tong, H. F.; Chen, J.; Lu, Y. M.; Yang, T. Q.; Yao X.; He, Y. B. High Recoverable Energy Density Over A Wide Temperature Range in Sr Modified $(Pb,La)(Zr,Sn,Ti)O_3$ Antiferroelectric Ceramics with An Orthorhombic Phase. Appl. Phys. Lett. **2016**, 109, 262901.

(21) Yang, Z.; Du, H.; Qu, S.; Hou, Y.; Ma, H.; Wang, J.; Wang, J.; Wei, X.; Xu, Z. Significantly Enhanced Recoverable Energy Storage Density in Potassium-Sodium Niobate-Based Lead Free Ceramics. J. Mater. Chem. A **2016**, 4, 13778-13785.

(22) Shao, T.; Du, H.; Ma, H.; Qu, S.; Wang, J.; Wang, J.; Wei, X.; Xu, Z. Potassium-Sodium Niobate Based Lead-Free Ceramics: Novel Electrical Energy Storage Materials. J. Mater. Chem. A **2017**, 5, 554-563.

(23) Liu, B. B.; Wang, X. H.; Zhao, Q. C.; Li, L. T. Improved Energy Storage Properties of Fine-Crystalline $BaTiO_3$ Ceramics by Coating Powders with Al_2O_3 and SiO_2. J. Am. Ceram. Soc. **2015**, 98, 2641-2646.

(24) Zhang, Q.; Wang, L.; Luo, J.; Tang, Q.; Du, J. $Ba_{0.4}Sr_{0.6}TiO_3$/MgO Composites with Enhanced Energy Storage Density and Low Dielectric Loss for Solid-State Pulse-Forming Line. Int. J. Appl. Ceram. Technol. **2010**, 7, E124-E128.

(25) Huang, Y. H.; Wu, Y. J.; Qiu, W. J.; Li, J. Chen, X. M. Enhanced Energy Storage Density of $Ba_{0.4}Sr_{0.6}TiO_3$-MgO Composite Prepared by Spark Plasma Sintering. J. Eur. Ceram. Soc. **2015**, 35,1469-1476.

(26) Ogihara, H.; Randall, C. A.; Trolier-McKinstry, S. High-Energy Density Capacitors Utilizing $0.7BaTiO_3$-$0.3BiScO_3$ Ceramics. J. Am. Ceram. Soc. **2009**, 92, 1719-1724.

(27) D. Wang, Z. Fan, D. Zhou, A. Khesro, S. Murakami, A. Feteira, Q. Zhao, X. Tan, I.M. Reaney, Bismuth ferrite-based lead-free ceramics and multilayers with high recoverable energy density. J. Mater. Chem. A **2018**, 6, 4133-4144.

(28) Shen, Z.; Wang, X.; Luo, B.; Li, L. T. $BaTiO_3$-$BiYbO_3$ Perovskite Materials for Energy Storage Applications. J. Mater. Chem. A **2015**, 3, 18146-18153.

(29) Wu, L.; Wang, X.; Li, L. Lead-Free $BaTiO_3$-$Bi(Zn_{2/3}Nb_{1/3})O_3$ Weakly Coupled Relaxor Ferroelectric Materials for Energy Storage. RSC Adv. **2016**, 6, 14273-14282.

(30) Zhao, X.; Zhou, Z.; Liang, R.; Liu, F.; Dong, X. High-Energy Storage Performance in Lead-Free $(1-x)BaTiO_3$-$xBi(Zn_{0.5}Ti_{0.5})O_3$ Relaxor Ceramics for Temperature Stability Applications. Ceram. Int. **2017**, 43, 9060-9066.

(31) Wang, T.; Jin, L.; Li, C.; Hu, Q.; Wei, X. Relaxor Ferroelectric $BaTiO_3$-$Bi(Mg_{2/3}Nb_{1/3})O_3$ Ceramics for Energy Storage Application. J. Am. Ceram. Soc. **2015**, 98, 559-566.

(32) Hu, Q.; Jin, L.; Wang, T.; Li, C.; Xing, Z.; Wei, X. Dielectric and Temperature Stable Energy Storage Properties of $0.88BaTiO_3$-$0.12Bi(Mg_{1/2}Ti_{1/2})O_3$ Bulk Ceramics. J. Alloys Comp. **2015**, 640, 416-420.

(33) Li, W. B.; Zhou, D.; Pang, L. X.; Xu, R.; Guo, H. H. Novel Barium Titanate Based Capacitors with High Energy Density and Fast Discharge Performance. J. Mater. Chem. A **2017**, 5, 19607-19612.

(34) Li, W. B.; Zhou, D.; Pang, L. X. Enhanced Energy Storage Density by Inducing Defect Dipoles in Lead Free Relaxor Ferroelectric $BaTiO_3$-Based Ceramics. Appl. Phys. Lett. **2017**, 110, 132902.

(35) Li, W. B.; Zhou, D.; He, B.; Li, F.; Pang, L. X.; Lu, S. G. Structure and Dielectric Properties of $Nd(Zn_{1/2}Ti_{1/2})O_3$-$BaTiO_3$ Ceramics for Energy Storage Applications. J. Alloys Comp. **2016**, 685, 418-422.

(36) Shannon, R. D. Dielectric Polarizabilities of Ions in Oxides and Fluorides. *J. Appl. Phys.* **1993**, 73, 348-366.

(37) Wei, M.; Zhang, J.; Wu, K.; Chen, H.; Yang, C. Effect of $BiMO_3$ (M=Al, In, Y, Sm, Nd, and La) Doping on The Dielectric Properties of $BaTiO_3$ Ceramics. *Ceram. Int.* **2017**, 43, 9593-9599.

(38) Xu, R.; Xu, Z.; Feng, Y.; Wei, X.; Tian, J.; Huang, D. Polarization of Antiferroelectric Ceramics for Pulse Capacitors Under Transient Electric Field. J. Appl. Phys. **2016**, 119, 224103.

(39) Xu, R.; Xu, Z.; Feng, Y.; Wei, X.; Tian, J.; Huang, D. Evaluation of Discharge Energy Density of Antiferroelectric Ceramics for Pulse Capacitors. Appl. Phys. Lett. **2016**, 109, 032903.

(40) Liu, B.; Wang, X.; Zhang, R.; Li, L. Energy Storage Properties of Ultra Fine-Grained $Ba_{0.4}Sr_{0.6}TiO_3$-Based Ceramics Sintered at Low Temperature. J. Alloys Comp. **2017**, 691, 619-623.

(41) Wu, L.; Wang, X.; Li, L. Core-Shell $BaTiO_3$@$BiScO_3$ Particles for Local Graded Dielectric Ceramics with Enhanced Temperature Stability and Energy Storage Capability. J. Alloys Comp. **2016**, 688, 113-121.

(42) Yang, H.; Yan, F.; Lin, Y.; Wang, T.; Wang, F. High Energy Storage Density Over A Broad Temperature Range in Sodium Bismuth Titanate-Based Lead-Free Ceramics. Sci. Rep. **2017**, 7, 8726.

(43) Yang, H.; Yan, F.; Lin, Y.; Wang, T.; Wang, F.; Wang, Y.; Guo, L.; Tai, W.; Wei, H. Lead-Free $BaTiO_3$-$Bi_{0.5}Na_{0.5}TiO_3$-$Na_{0.73}Bi_{0.09}NbO_3$ Relaxor Ferroelectric Ceramics for High Energy Storage. J. Eur. Ceram. Soc. **2017**, 37, 3303-3311.

(44) Chen, P.; Chu, B. Improvement of Dielectric and Energy Storage Properties in $Bi(Mg_{1/2}Ti_{1/2})O_3$-Modified $(Na_{1/2}Bi_{1/2})_{0.92}Ba_{0.08}TiO_3$ Ceramics. J. Eur. Ceram. Soc. **2016**, 36, 81-88.

(45) Liu, Z.; Ren, P.; Long, C.; Wang, X.; Wan, Y.; Zhao, G. Enhanced Energy Storage Properties of $NaNbO_3$ and $SrZrO_3$ Modified $Bi_{0.5}Na_{0.5}TiO_3$ Based Ceramics. J. Alloys Comp. **2017**, 721, 538-544.

(46) Luo, L.; Wang, B.; Jiang, X.; Li, W. Energy Storage Properties of $(1-x)(Bi_{0.5}Na_{0.5})TiO_3$-$xKNbO_3$ Lead-Free Ceramics. J. Mater. Sci. **2014**, 49, 1659-1665.

(47) Wang, B.; Luo, L.; Jiang, X.; Li, W.; Chen, H. Energy-Storage Properties of $(1-x)Bi_{0.47}Na_{0.47}Ba_{0.06}TiO_3$-$xKNbO_3$ Lead-Free Ceramics. J. Alloys Comp. **2014**, 585, 14-18.

(48) Gao, F.; Dong, X.; Mao, C.; Liu, W.; Zhang, H.; Yang, L.; Cao, F.; Wang, G. c/a Ratio-Dependent Energy-Storage Density in $(0.9-x)Bi_{0.5}Na_{0.5}TiO_3$-$xBaTiO_3$-$0.1K_{0.5}Na_{0.5}NbO_3$ Ceramics. J. Am. Ceram. Soc. **2011**, 94, 4162-4164.

(49) Borkar, H.; Singh, V. N.; Singh, B. P.; Tomar, M.; Gupta, V.; Kumar, A. Room Temperature Lead-Free Relaxor-Antiferroelectric Electroceramics for Energy Storage Applications. RSC adv. **2014**, 4, 22840-22847.

(50) Tian, Y.; Jin, L.; Zhang, H.; Xu, Z.; Wei, X.; Politova, E. D.; Stefanovich, S. Y.; Tarakina, N. V.; Abrahams, I.; Yan, H. High Energy Density in Silver Niobate Ceramics. J. Mater. Chem. A **2016**, 4, 17279-17287.

(51) Wu, J.; Mahajan, A.; Riekehr, L.; Zhang, H.; Yang, B.; Meng, N.; Zhang, Z.; Yan, H. Perovskite $Sr_x(Bi_{1-x}Na_{0.97-x}Li_{0.03})_{0.5}TiO_3$ Ceramics with Polar Nano Regions for High Power Energy Storage. Nano Energy **2018**, 50, 723-732.

(52) Sun, Z.; Ma, C.; Wang, X.; Liu, M.; Lu, L.; Wu, M.; Lou, X.; Wang, H.; Jia, C. L. Large Energy Density, Excellent Thermal Stability, and High Cycling Endurance of Lead-Free $BaZr_{0.2}Ti_{0.8}O_3$ Film Capacitors. ACS Appl. Mater. Interfaces **2017**, 9, 17096-17101.

(53) Wang, D.; Fan, Z.; Li, W.; Zhou, D.; Feteira, A.; Wang, G.; Murakami, S.; Sun, S.; Zhao, S.; Tan, X.; Reaney, I. M. High Energy Storage Density and Large Strain in $Bi(Zn_{2/3}Nb_{1/3})O_3$-Doped $BiFeO_3$-$BaTiO_3$ Ceramics. ACS Appl. Energy Mater. **2018**, DOI: 10.1021/acsaem.8b01099.

Table of Contents (TOC)